PLASMA DYNAMICS

XII. PLASMA DYNAMICS

Academic and Research Staff

Prof. William P. Allis
Prof. Abraham Bers
Prof. George Bekefi
Prof. Sanborn C. Brown
Prof. Sow-Hsin Chen
Prof. Bruno Coppi
Prof. Thomas H. Dupree
Prof. E. Victor George
Prof. Elias P. Gyftopoulos
Prof. Hermann A. Haus

Prof. Lawrence M. Lidsky
Prof. James E. McCune
Prof. Peter A. Politzer
Prof. Dieter J. Sigmar
Prof. Louis D. Smullin
Prof. Robert J. Taylor
Prof. Sidney Yip
Dr. Edward G. Apgar
Dr. Giuseppe F. Bosia
Dr. Philippe Brossier

Dr. Bert C. J. M. DeKock
Dr. Bernard J. Meddens
Dr. D. Bruce Montgomery*
Dr. Lodewyk T. M. Ornstein
Dr. Ronald R. Parker
Dr. Roberto Pozzoli
Dr. Arthur H. M. Ross
Dr. Piet van der Laan
John J. McCarthy
William J. Mulligan

Graduate Students

Eugene L. Bernstein
Charles T. Breuer
Leslie Bromberg
Natale M. Ceglio
Frank W. Chambers
Hark C. Chan
Tsi-Pin Choong
Wing-Shek Chow
Paul W. Chrisman, Jr.
Donald L. Cook
David A. Ehst
Nathaniel J. Fisch
Jay L. Fisher
Alan R. Forbes
Ricardo M. O. Galvão
Keith C. Garel
Jeffry Golden
Richard J. Hawryluk

Ady Hershcovitch
Steven P. Hirshman
James C. Hsia
Donald P. Hutchinson
Saeed Z. Jabbawy
Charles F. F. Karney
David S. Komm
John L. Kulp, Jr.
Ping Lee
Yongyut Manichaikul
Paul M. Margosian
François Martin
John L. Miller
Paul E. Morgan
Michael R. Murphy
Thaddeus Orzechowski
David O. Overskei
Aniket Pant

Louis R. Pasquaretti
Gerald D. Pine
Robert H. Price
Charles A. Primmerman
Donald Prosnitz
Gregory Rewoldt
Paul A. Roth
Mario Simonutti
Miloslav S. Tekula
David J. Tetrault
Alan E. Throop
Marcio L. Vianna
Bruce V. Waddell
Yi-Ming Wang
Duncan C. Watson
Charles W. Werner
David M. Wildman
Stephen M. Wolfe

---

*Dr. Bruce Montgomery is at the Francis Bitter National Magnet Laboratory.

XII. PLASMA DYNAMICS

A. Experimental Studies — Waves, Turbulence, and Radiation

1. LINEAR WAVE CONVERSION OF RESONANCE CONES NEAR LOWER HYBRID RESONANCE

Mario Simonutti

Introduction

In Quarterly Progress Report No. 113 (pp. 93-104) we described a derivation, based on the moment equations for electrons and ions in the electrostatic approximation and without collisions, of the differential equation governing linear mode conversion of a single k_z wave in an inhomogeneous magnetized plasma near lower hybrid resonance (LHR). We also explained a technique for obtaining a numerical solution to this system and presented a typical solution.

In this report we shall describe the numerical Fourier synthesis of a discrete spectrum of those single k_z wave solutions. This process yields a solution to the problem of describing the behavior of resonance cones[1,2] near LHR in an inhomogeneous plasma with thermal effects included. This solution displays the pronounced influence of mode conversion on the resonance cones.

RF Coupling Model

In the model for the single k_z wave numerical solutions obtained in this work, RF power couples from a boundary of imposed potential $\Phi \exp(i(\omega t - k_z z))$ located in the low-density region at $x = 0$. That boundary potential was taken to couple fully to the ingoing (in the x-directed group velocity sense) long-wavelength cold-plasma mode, while the amplitude of the ingoing short-wavelength warm-plasma mode was set identically to zero. There were two reasons for the choice of this model. First, an antenna structure located at the low-density edge of a plasma couples more readily to a mode whose wavelength is closer to the vacuum wavelength range. Also, any excitation of the ingoing short-wavelength mode damps out close to the antenna well before reaching the main body of the plasma.

In the numerical solution the presence of the outgoing long-wavelength mode is determined by the differential equation. In general, it must be treated explicitly in the coupling model. Except in extreme cases of small k_z and/or small density profile scale lengths, however, the numerical solution shows that this component is present in negligible proportions. This result leads us to the important conclusion that complete conversion from the cold-plasma mode to the warm-plasma mode takes place. Therefore the outgoing long-wavelength mode need not enter at all into the coupling problem, and we may neglect it in the coupling model.

It can be expected that an imposed driving potential $\Phi(z)$ exp(iωt) located at x = 0 and spatially localized in the z direction will launch cold-plasma resonance ˙cones which, upon reaching the conversion region at higher plasma densities, will be transformed to a warm-plasma type of oscillation.

The final processing for each single k_z wave solution produced is a normalization such that the contribution to the total potential Φ from the ingoing long-wavelength mode at the boundary x = 0 (where the driving potential source is located) has unity amplitude and zero phase angle. This qualifies the response as that driven by a source of Φ of unity amplitude and zero phase angle.

Individual Components of the k_z Spectrum

A set of parameters is chosen to describe the plasma and RF driving source to be modeled by the numerical problem. These parameters are given in Figs. XII-1, XII-2, and XII-3. Although most parameters are dimensionless, a practical experimental situation to which these results might apply would have the frequency of operation at ~40 MHz = ω/2π. A relatively high magnetic field case was treated in an attempt to minimize finite $k_x a_i$ (perpendicular wave number times the ion Larmor radius) effects under which the moment equation theory, upon which our work is based, may be of questionable validity.

We are now making a comparison of numerical solutions of the two dispersion relations that follow from moment equation theory and from the hot-plasma theory through the Harris dispersion relation.[4] Preliminary results indicate that the two theories are in close agreement in their general description of the k_x vs density branches characterizing the phenomenon of wave conversion near LHR, even when $k_x a_i$ exceeds unity by a considerable factor. Therefore the moment equation theory should be valid in this treatment, and the magnetic field need not have been chosen so high in this particular case.

The density profile taken is shown in Fig. XII-1 and two single k_z wave solutions for some of the variables are presented in Fig. XII-2. A series of such solutions makes up the spectrum of the resonance cone response. Figure XII-1 shows different upper level density plateaus for the range of n_z (=$k_z c/ω$) used in the numerical solutions for the resonance cone. Larger n_z implies a decreased mode conversion density. As n_z is increased, a lower density plateau is taken together with a smaller x starting value on that plateau in order to avoid numerical swamping in the regions where the solution has exponential character. Care is taken to ensure that the solution decays several orders of magnitude on the finite slope of the linear portion before the break to the level density plateau is made. Although the individual n_z wave solutions are for density profiles that differ in this manner, the actual solutions for densities near and less than the mode conversion density should be insensitive to such changes in the density profile.
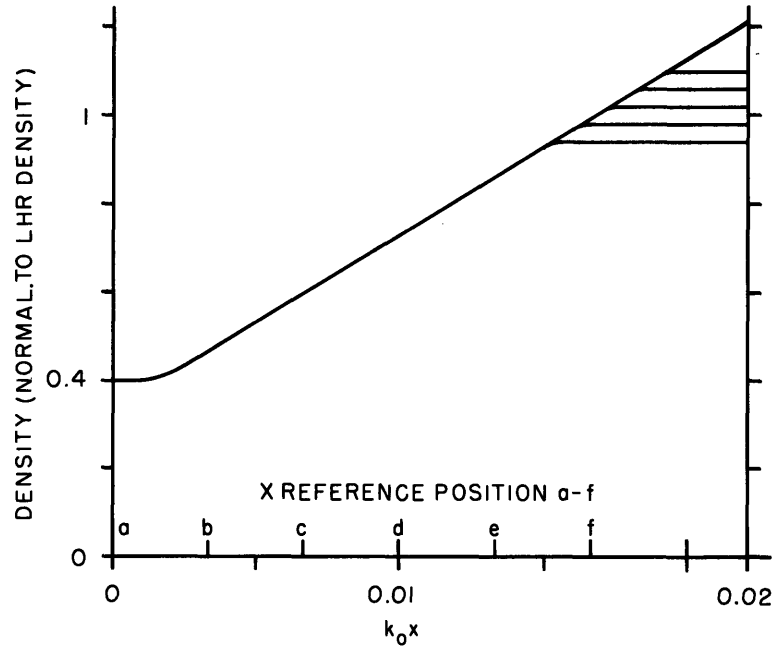
103

Fig. XII-1. Density profiles for the numerically generated n_z
component solutions. Equally spaced x reference
positions from x = a to x = f are indicated.

Several general and important points should be noted in the solutions shown in
Fig. XII-2. First, a mild maximum is displayed in the mode conversion region. Second,
the conversion density decreases for increased n_z. Third, before the conversion density,
the solutions comprise an interference of two traveling waves of differing phase velocity,
and the phase velocities are both directed toward lower density. Fourth, each variable
has a different x-dependence. Fifth, the RF phase plots indicate that Φ is made up
mainly of the long-wavelength ingoing mode (a backward wave), while some other vari-
ables are made up mainly of the warm-plasma mode which indicates that the nature of the
outgoing mode is acoustic or mechanical, rather than electrical. This will be displayed
in the resonance cone solutions.

The second and third points can be predicted by arguments based only upon the n_x
wave number vs density plots for these modes and on an a priori assumption of complete
conversion. The fourth and fifth points can be predicted by these arguments, plus con-
siderations of the complex small-signal conservation theorem and of the eigenvectors
of the two modes of interest (see our report in Quarterly Progress Report No. 113). The
first point follows from the actual solution of the differential equation.

Wave Conversion of the Resonance Cones

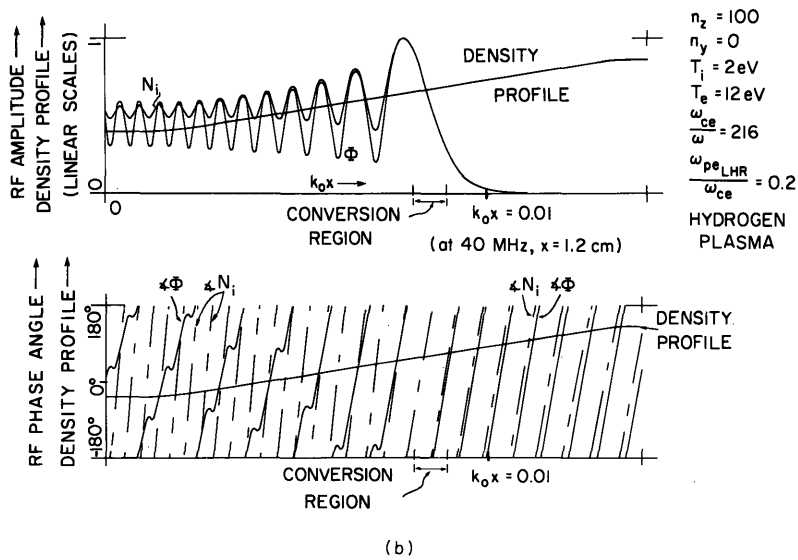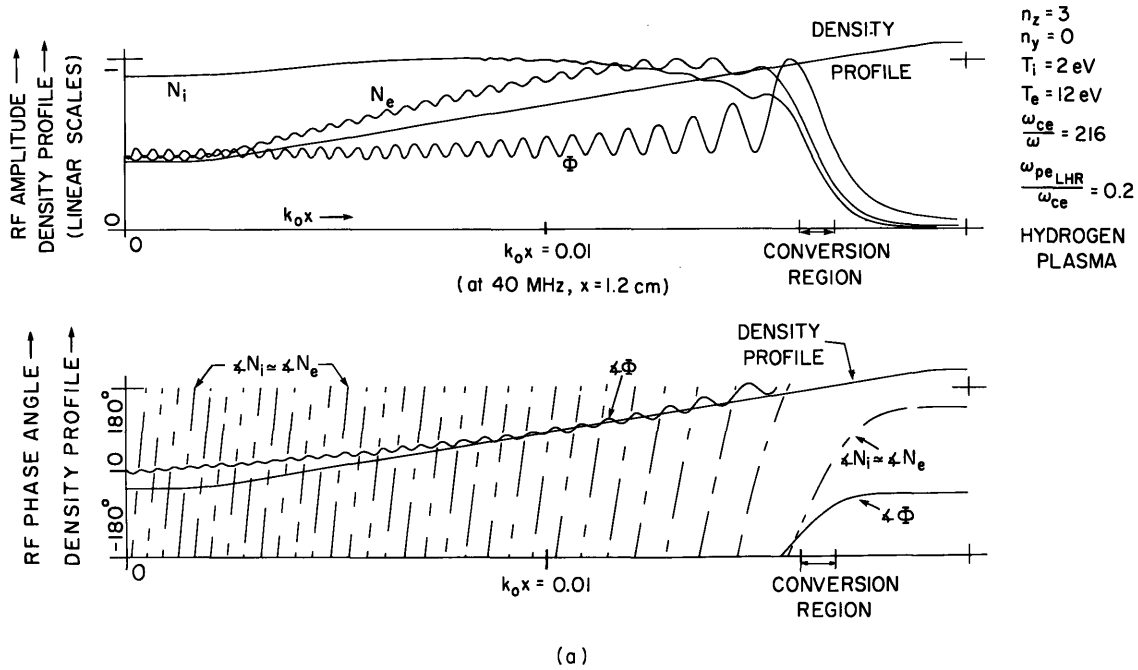In order to perform a discrete Fourier synthesis of a spectrum of these n_z wave

Fig. XII-2. RF amplitude (linear scale) and phase of single n_z wave solutions for several variables and for 2 values of imposed n_z: (a) $n_z = 3$, (b) $n_z = 100$.

solutions, we must choose the n_z spacing and maximum n_z value. This then determines the number of discrete n_z components to be generated. The n_z spacing of these discrete components determines the periodicity in z space of the resulting transform. This periodicity length should be somewhat greater than the estimated z extent covered by the ingoing resonance cones and outgoing converted oscillations. A guideline for the ratio of z extent to x distance to the LHR region[2] is the square root of the mass ratio, $(m_i/m_e)^{1/2}$; a safety factor approximately three times this is taken. The choice of the maximum n_z value is determined by two factors: the regime for electron Landau damping parallel to the magnetic field when $k_z v_{te}/\omega$ approaches unity should be avoided, and as the z extent of the driving source, spatially localized in z, is reduced higher n_z components must be included.

We took 101 components with n_z running from -60 to $+60$ and spaced by $n_z = 1.2$. Note that relatively large n_z values are included because relatively low values for T_e and T_i are taken and the intended operating frequency is low (~40 MHz) in order to model a small-scale laboratory experimental arrangement. Since the component solutions are even in n_z, only the positive n_z components had to be generated numerically. The $n_z = 0$ solution was set identical to zero to account for the lack of accessibility[4] for that component.

If each of the 101 components constituting the driving source spectrum were taken with equal amplitude, nonphysical oscillations in the z-space solutions would be introduced in the discrete Fourier transform (DFT) process. In order to avoid this kind of oscillation, an appropriate smoothing window function was taken.

$$W(N) = .5 \ (1 + \cos(\pi N/51)).$$

Each of the 101 n_z components centered about $n_z = 0$ and numbered from N = -50 to N = $+50$ were multiplied by this function.

Results for four of the physical variables are presented in Fig. XII-3 in terms of the RF amplitude and phase of the solutions as a function of z at the x reference positions shown in Fig. XII-1. Since the solutions are even functions of z, only positive z is shown. With 40-MHz operation, the extent of these distance scales would be 3.1 m in z, 1.67 cm in x. This large difference is a result of the nature of the variation with density of the cold-plasma resonance cone angle near LHR.

Figure XII-3a shows the solution for $\Phi(x, z)$. The x = 0 plot (position a) near z = 0 shows the form of the driving source potential, an excitation localized in z (~20 cm wide at 40 MHz). As x increases, this pulse splits into 2 pulses of approximately half peak amplitude. Only the pulse directed toward increasing z is shown. It travels toward higher density at a varying angle with respect to the magnetic field which is directed along z. The dependence of this angle on density is characteristic of the cold-plasma resonance cones. Wave conversion converts this to an oscillation directed perpendicular
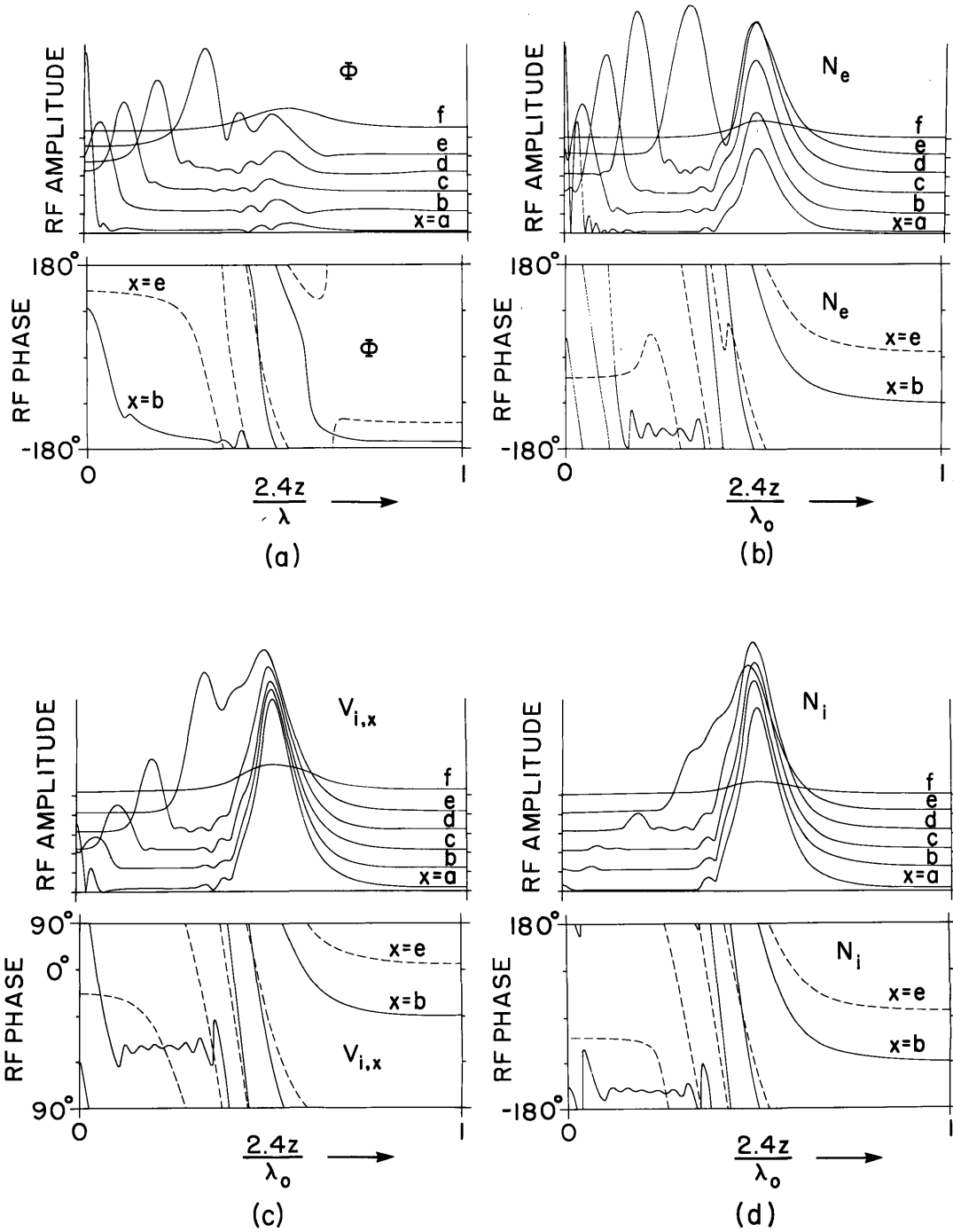
Fig. XII-3. RF amplitude of resonance cone solutions for 4 variables, for 6 reference positions; and RF phase for 2 x-reference positions. Plasma parameters, same as in Fig. XII-2: (a) Φ, (b) N_e, (c) $v_{i,x}$, (d) N_i.

to the magnetic field and back out of the plasma. For the Φ solution, this oscillation has reduced amplitude compared with the ingoing cone. For the ion RF density N_i, however, and for the ion x component of RF velocity $V_{i,x}$, the amplitude of the outgoing oscillation increases. This follows from the acoustic nature of this oscillation generated by mode conversion and from the conservation of small-signal power which this theory demands.

Conclusion

Some of the basic characteristics of the influence of wave conversion on resonance cones as described by these numerical solutions can be explained readily by basic considerations of the dispersion relations, the small-signal conservation theorem, the assumption of complete conversion, and so forth. Some important details such as the nature of the solutions in the conversion region and of the outgoing oscillation have not been predicted previously. The numerical solutions presented here should be useful in providing a clear understanding of the interesting physical concepts involved in this problem. The numerical techniques should be valuable in providing quantitative information for the design of an experiment that might provide direct evidence of the wave conversion process through resonance cone measurements, and for the design of LHR plasma-heating systems.

The limitations of this theory must be kept in mind. No dissipative process such as collisions has been included. Also, the outgoing mode will not actually reach the low-density outside edge of the plasma. It will undergo further transformation dictated by hot-plasma theory.

References

1. R. K. Fisher and R. W. Gould, Phys. Fluids **14**, 857 (1971).

2. R. J. Briggs and R. R. Parker, Phys. Rev. Letters **29**, 852 (1972).

3. T. H. Stix, The Theory of Plasma Waves (McGraw-Hill Publishing Co., New York, 1962), p. 225.

4. Ibid., pp. 60-65.

2. INVESTIGATION OF THE TRAPPED ELECTRON SCATTERING MODE IN CYLINDRICAL GEOMETRY

Charles A. Primmerman, Lawrence M. Lidsky, Peter A. Politzer

Introduction

In toroidal geometry the existence of a class of trapped particles executing "banana orbits" has a profound effect on plasma response, resulting in a whole new class of unstable oscillations.[1] One such instability is the trapped electron scattering mode first derived by Coppi,[2] and investigated by Coppi and Rewoldt.[3] This mode is driven by resonant interaction with trapped electrons and has a potential profile singularly well suited to the scattering of deeply trapped particles, hence the appellation "scattering mode." It is difficult to investigate this mode in present Tokamaks; thus, we have investigated it in cylindrical geometry. The advantage in using cylindrical geometry is that collisionless plasmas may be produced easily in linear laboratory devices. Moreover, the study of waves can be accomplished more easily in low-temperature linear machines than in Tokamaks. The disadvantage with cylindrical geometry is that the theory must be carefully reworked to confirm that the mode exists in both cylindrical and toroidal geometry. First, we shall develop the cylindrical geometry analog to the toroidal trapped electron scattering mode. Second, we shall report experimental observations of this mode in cylindrical geometry.

Theory

We begin by postulating a cylindrical plasma confined by a spatially periodic magnetic field

$$\underline{B} = B_z = B_o\left(1 - \epsilon \cos \frac{2\pi z}{L}\right), \tag{1}$$

where ϵ is a small quantity, and L is the distance between mirrors. We consider the low β limit and look for electrostatic modes of the form

$$\tilde{\Phi} = \tilde{\phi}_m(z) \exp(im\theta - i\omega t), \tag{2}$$

where $\tilde{\phi}_m(z)$ is a periodic function of z depending on the magnetic-field period. In particular, we specialize to the case $\tilde{\phi}_m(z)$ odd about the magnetic-field minimum. This choice is not merely a mathematical convenience; it has important physical consequences. For, while the mathematical formalism is applicable to both odd and even periodicity, the two different periodicities result in modes with quite different properties.

We find that only for odd modes will unstable oscillations exist at frequencies comparable to the electron bounce frequency fundamental.

We consider parameters such that $T_e \gg T_i$; $\omega \gg \Omega_i$; $\omega \gg \frac{\pi}{L}(T_i/m_i)^{1/2}$. For these parameters the ion bounce motion may be neglected, and the ions are effectively unmagnetized. The ion response may then be treated as an inertial response to the fluctuating electric field

$$m_i \frac{d\tilde{v}_i}{dt} = -e\nabla\tilde{\Phi}. \tag{3}$$

Using $\frac{\partial n}{\partial t} + \nabla \cdot (n\underline{v}) = 0$ and $\nabla^2\tilde{\Phi} \approx -\frac{m^2}{r^2}\tilde{\Phi}$, we have

$$\tilde{n}_i = \frac{n_i e}{m_i \omega^2} \frac{m^2}{r^2} \tilde{\Phi}. \tag{4}$$

The perturbed electron density may be found in the standard manner by integrating the linearized Vlasov equation along the unperturbed particle orbits. We consider the frequency range

$$\nu_{eff} \stackrel{<}{{}} \omega_{De} \ll \omega \stackrel{<}{\sim} \langle \omega_{be} \rangle \sim \omega_{*e} \ll \Omega_e, \tag{5}$$

where ν_{eff} is the effective collision frequency for detrapping collisions $\nu_{eff} = \frac{\nu_{en}}{\epsilon}$; ω_{De} is the magnetic drift frequency $\omega_{De} = \frac{m}{r}\left(\frac{1}{2}v_\perp^2 + v_\parallel^2\right)\frac{m_e\nabla B}{qB^2}$; $\langle \omega_{be} \rangle$ is the average bounce frequency; ω_{*e} is the diamagnetic drift frequency $\omega_{*e} = \frac{-mT_e}{reBn_e}\frac{dn_e}{dr}$; and Ω_e is the electron cyclotron frequency. We take the unperturbed distribution function to be locally Maxwellian with both density and temperature functions of radius

$$f_{oe} = \frac{n_e(r)}{(2\pi T_e(r)/n_e)^{3/2}} \exp[-\mathscr{E}/T_e(r)]. \tag{6}$$

Using these assumptions and neglecting finite Larmor radius effects, we follow Horton et al.[4] to obtain

$$\tilde{n}_e = \frac{en_e}{T_e}\left[\tilde{\Phi} - \frac{1}{n_e}\int d^3\underline{v}\, f_{oe}\left(\omega - \omega_{*e}^T\right) I(t)\right], \tag{7}$$

where

$$I(t) = i \int_{-\infty}^{t} dt' \; \tilde{\Phi} \; \exp[-i\omega(t'-t)]$$

$$\omega_{*e}^{T} = \omega_{*e}\left[1 + \eta\left(\mathscr{E}/T_e - \frac{3}{2}\right)\right]$$

$$\omega_{*e} = \frac{-mT_e}{reB} \frac{1}{n_e} \frac{dn_e}{dr}$$

$$\eta = \frac{d \ln T_e}{d \ln n_e}.$$

The time integral may be done formally by expanding $\tilde{\phi}_m(z)$ in terms of bounce fre-quency harmonics for trapped particles and transit frequency harmonics for circulating particles. Upon performing this expansion we obtain resonant terms of the form $\frac{1}{\omega - p\omega_{be}}$, where, for odd modes, $p = 1, 3, 5, \ldots$. In contrast, for even modes p must be even. Thus we have the result that for odd modes the primary resonance is with par-ticles which have bounce frequencies equal to the wave frequency, while for even modes resonance is possible only for harmonics of the bounce frequency.

We continue by substituting the expressions for $\tilde{n}_i$ and $\tilde{n}_e$ in Poisson's equation $-\nabla^2\tilde{\Phi} = \frac{e}{\epsilon_o} (\tilde{n}_i - \tilde{n}_e)$, and by operating with $\int_{-L/2}^{L/2} \frac{dz}{B_z} \tilde{\Phi}^*(z)$, to get a quadratic form. The resulting equation has no simple analytic expression except when $\omega \ll \omega_{*e}$, $\langle \omega_{be} \rangle$. If we examine this low-frequency limit and make the additional assumptions $\lambda_{De} = 0$, $m_i \to \infty$, the quadratic form reduces to

$$\psi_1 + \frac{\omega_{*e}\omega(\eta-1)}{4\pi^2\epsilon^{3/2}\bar{\omega}_{te}^2} \; \psi_2 + \frac{i\sqrt{\pi} \; \omega^2\omega_{*e}\left(\frac{3}{2}\eta-1\right)}{8\pi^3\epsilon^2\bar{\omega}_{te}^3} \; \psi_3 = 0, \tag{8}$$

where $\bar{\omega}_{te}$ is the average transit frequency defined by $\bar{\omega}_{te} = \frac{\pi}{L} (2T_e/m_e)^{1/2}$ and ψ_1, ψ_2, ψ_3 are positive definite integrals. By taking $\omega = \omega_r + i\gamma$; $\gamma \ll \omega_r$, Eq. 8 yields

$$\omega_r = \frac{4\pi\epsilon^{3/2}\bar{\omega}_{te}^2}{(1-\eta)\omega_{*e}} \frac{\psi_1}{\psi_2}$$

$$\gamma = \frac{\left(\frac{3}{2}\eta-1\right)\omega_r^2}{(1-\eta) \, 2\sqrt{\pi} \, \epsilon^{1/2}\bar{\omega}_{te}} \frac{\psi_3}{\psi_2}. \tag{9}$$

Computation of the integrals ψ_1, ψ_2, ψ_3 reveals that Eqs. 9 do, in fact, satisfy the assumed inequalities $\omega_r \ll \omega_{*e}$, $\langle \omega_{be} \rangle$ and $\gamma \ll \omega_r$. For instability we must have $\gamma > 0$, which requires

$$\frac{2}{3} < \eta < 1. \tag{10}$$

This instability condition is the same as that obtained by Coppi in toroidal geometry. But, although this low-frequency result is attractive because of its simplicity, its practical usefulness is suspect. We have noted that this mode is driven by resonance with particles that have bounce frequencies at the wave frequency; thus, we expect that the waves with largest growth rates will occur for $\omega \approx \langle \omega_{be} \rangle$, not for $\omega \ll \langle \omega_{be} \rangle$. The low-frequency result itself confirms the view that the low-frequency oscillations are least important, since the dependence of the growth rate on the real frequency is $\gamma \propto \omega_r^2$. An additional problem with our low-frequency result is that to obtain it we have ignored the important effect of noninfinite ion inertia.

To obtain more physically meaningful theoretical predictions, we have solved the equations numerically, including the effects of finite λ_{De} and m_i. The results of this numerical solution are shown graphically in Fig. XII-4, where we have plotted γ against ω_r for fixed η (solid curves) and for fixed ω_{*e} (dashed curves) for three different values of ϵ. All frequencies have been normalized to $\bar{\omega}_{te}$ the average transit frequency. We note that all three sets of curves exhibit similar behavior: for the usual situation in which n and T decrease with increasing r so that $\eta > 0$ we see that there is a small region of unstable frequencies. As ϵ increases, this instability region shifts to higher real frequencies and larger growth rates. This behavior is easy to explain qualitatively. We expect that the real frequency will be $\omega \approx \langle \omega_{be} \rangle$ and since $\langle \omega_{be} \rangle \approx \sqrt{2\epsilon}\,\bar{\omega}_{te}$, the real frequency should be proportional to $\sqrt{\epsilon}$. We might expect also that the growth rate would somehow be directly related to the fraction of trapped particles, which would make γ dependent on $\sqrt{\epsilon}$. We observe that the center frequency of the unstable band is slightly greater than $\langle \omega_{be} \rangle$, a result that is affected by the exact form of $\tilde{\phi}_m(z)$. For these curves we have used $\tilde{\phi}_m(z) = \sin \frac{2\pi z}{L}$. Since in a sinusoidal well the bounce frequency decreases as the turning point comes closer to B_{max}, we expect that $\tilde{\phi}_m(z)$ peaked closer to B_{max} will yield lower real frequencies. This expectation is confirmed by numerical computations. In all cases the maximum growth rate is small, $\gamma \lesssim .05\,\omega_r$, and occurs for $\eta \approx 0$.

Examining the family of curves for various ω_{*e}, we observe that the largest growth rates coincide with $\omega \approx \omega_{*e}$. Since we have not solved for the radial eigenmode, the matching of the two sets of curves in Fig. XII-4 determines the radial location of the instability. But, for the parameters of Fig. XII-4, chosen to approximate our
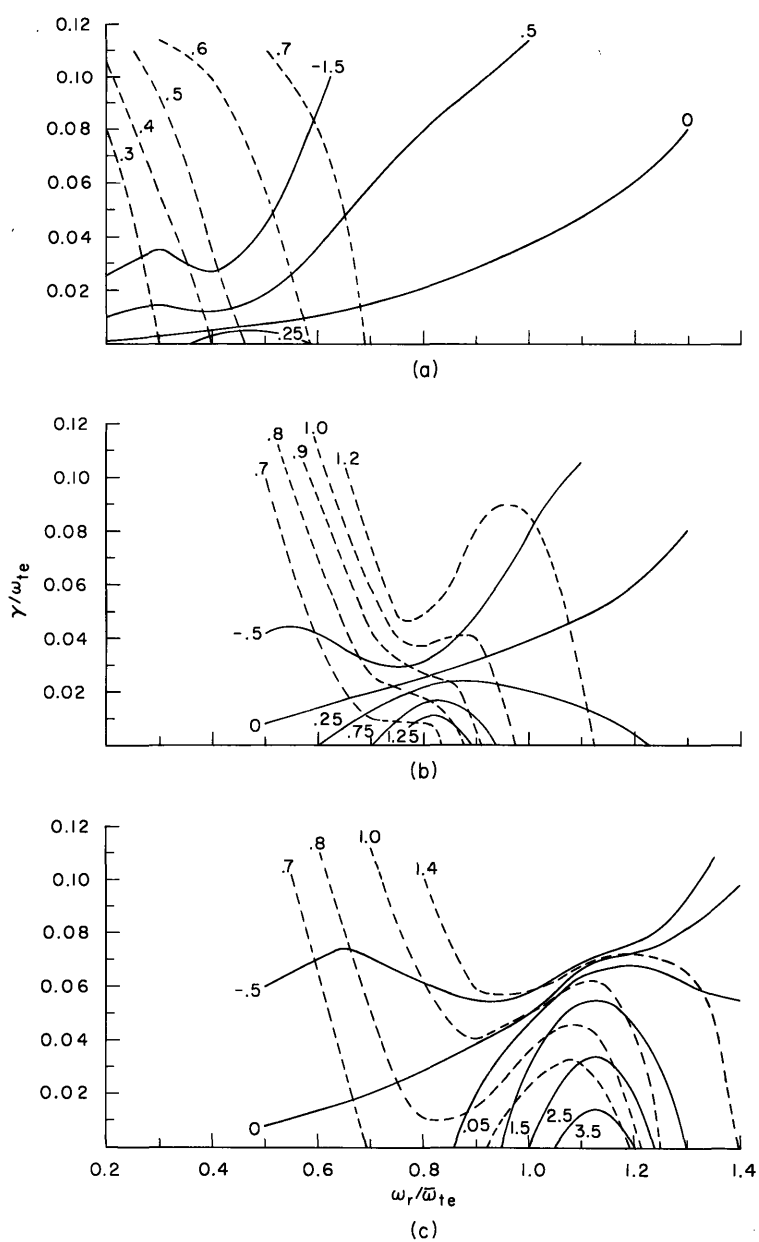
Fig. XII-4. Numerical solutions for growth rate γ vs real frequency ω_r, with η fixed (solid curves) and ω_{*e} fixed (dashed curves) for three values of ϵ. $B_z = B_0\left(1 - \epsilon \cos \frac{2\pi z}{L}\right)$; $\eta = \frac{d \ln T_e}{d \ln n_e}$; $\omega_{*e} = -\frac{m}{r} \frac{T_e}{eB} \frac{1}{n_e} \frac{dn_e}{dr}$. All frequencies are normalized to $\bar{\omega}_{te}$, where $\bar{\omega}_{te} = \frac{\pi}{L} (2T_e/m_e)^{1/2}$. Results are for an argon plasma with $T = 10$ eV; $n = 5 \times 10^{10}/\text{cm}^3$; and $\frac{1}{n}$ dn/dr = 2 cm^{-1} (a) $\epsilon = 0.05$. (b) $\epsilon = 0.15$. (c) $\epsilon = 0.25$.

experimental conditions, the high mode number implied by $\omega = \omega_{*e}$ vitiates the matching criterion: for almost any value of η we can find a mode number that allows $\omega = \omega_{*e}$. Thus we expect the frequency and radial location of the mode to be primarily determined by the η family of curves. To facilitate comparison with experimental results, the theoretical predictions for the trapped electron scattering mode in cylindrical geometry are summarized in Table XII-1.

Table XII-1.   Theoretical predictions for the cylindrical
trapped electron scattering mode.

1.	Frequency	$\omega \approx \omega_{*e} \approx \langle \omega_{be} \rangle$
2.	Dependence on Collision Frequency	Mode exists only for $\nu_{eff} < \omega$
3.	Azimuthal Variation	Propagates with electron diamagnetic drift veloc- ity $v_\theta \approx r\omega_{*e}/m$
4.	Radial Variation	Standing wave. Localized about $\eta \approx 0$
5.	Axial Variation	Standing wave. $\tilde{\phi}_m(z)$ odd about B_{min}
6.	Dependence on Trapping Well	$\omega_r \propto \sqrt{\epsilon}$ γ increases with increasing ϵ

Experiment

The experimental device is illustrated in Fig. XII-5. In uniform field operation 12 magnets produce a field of ~1 kG flat to within ~5%. To produce 4 concatenate trapping wells, 4 magnets are independently controlled to produce a field that can be reasonably approximated by $B_z = B_0\left(1 - \epsilon \cos \frac{2\pi z}{L}\right)$, where L = 0.5 m, and ϵ may be varied from 0 to 0.4. The main deviation of the field from sinusoidal is that the minima are somewhat broader than the maxima. The plasma is an RF discharge argon plasma produced by a Lisitano coil driven by 30 W of microwave power at 3 GHz. The plasma formed typically has $n \sim 10^{10}-10^{11}/cm^3$; $T_e \sim 5-10$ eV; $T_i \sim 0.2$ eV; $\frac{1}{n}\frac{dn}{dr} \sim$ 1-2 cm^{-1}. The ions are sufficiently collisional that they do not execute trapped particle orbits. The neutral pressure may be varied so that the electrons are either collisional or collisionless with respect to bounce frequency orbits. Since the flow out of the ends of the machine is limited by the slow ions, the end plates charge negatively; thus, the bulk of the electrons are confined electrostatically, making many transits
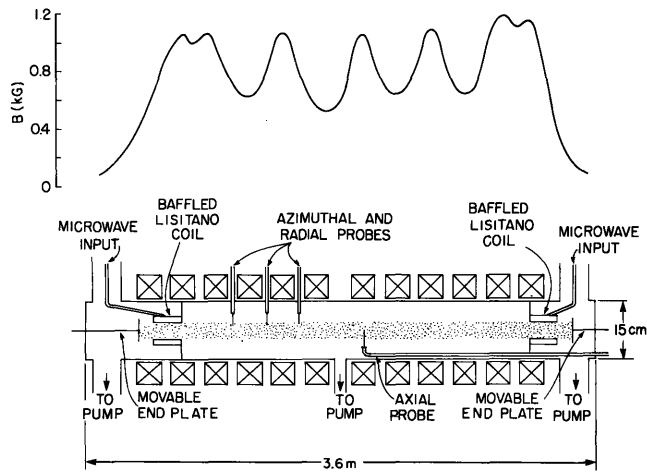
Fig. XII-5.

Schematic illustration of the experimental device with the periodic magnetic field shown for $\epsilon = 0.25$.
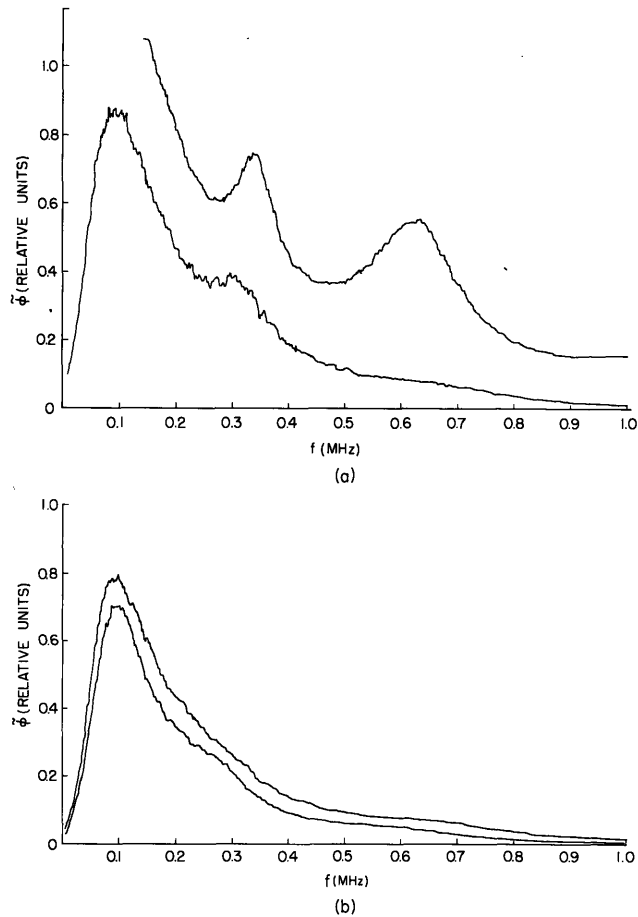

(a)

(b)

Fig. XII-6. (a) Potential fluctuation spectrum at low collision frequency. Upper curve: trapping well with $\epsilon = 0.2$. Lower curve: uniform field.
(b) Potential fluctuation spectrum at high collision frequency. Upper curve: trapping well with $\epsilon = 0.2$. Lower curve: uniform field.

of the machine before they are lost. These electrons form a good analogy to the circulating electrons in toroidal geometry.

At sufficiently low collision frequency we observe a dramatic change in the plasma noise spectrum upon the application of a trapping magnetic field. The situation is illustrated in Fig. XII-6a, where we have plotted the spectrum with and without a trapping well. The upper curve is for a trapping field with $\epsilon = 0.2$, $\langle \omega_{be} \rangle \approx 1$ MHz; the lower curve is for uniform field. We observe that for the trapping field case there is a tenfold increase in the noise level at frequencies near $\langle \omega_{be} \rangle$ and that a coherent mode appears at a frequency somewhat below $\langle \omega_{be} \rangle$. For comparison, we show the same curves in Fig. XII-6b at higher collision frequency. We see that the spectrum for the uniform field case has changed but little; while for the trapping-well case the noise enhancement near $\langle \omega_{be} \rangle$ has almost entirely disappeared. For still higher collision frequencies the spectra are identical.

The cutoff of the observed modes above a certain collision frequency is a very pronounced effect, as illustrated in Fig. XII-7. Here we have plotted amplitude at 650 kHz against pressure with and without a trapping well. We note that at the highest pressures the amplitudes are the same. As the pressure is lowered, the fluctuation level increases slightly for the uniform-field case, but for the trapping-well case the level rises sharply at a neutral pressure of $\sim 2 \times 10^{-5}$ Torr. Also noted on the curve is the pressure at which $\nu_{eff} = \omega$. We see that the wave amplitude rises sharply for $\nu_{eff}/\omega < 1/3$.
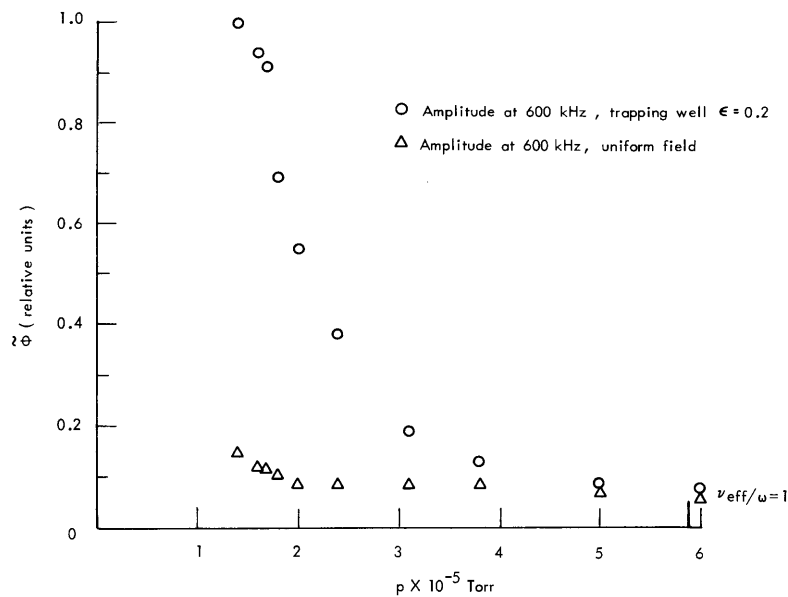
Fig. XII-7. Potential fluctuation of amplitude vs neutral gas pressure.

The results are similar for all values of ϵ above $\epsilon \approx 0.1$. We see typically one or more modes excited, with the primary mode at a frequency somewhat below $\langle \omega_{be} \rangle$. The oscillations are observed to decrease rapidly as the collision frequency becomes comparable to the wave frequency. The fact that the primary mode occurs for frequencies slightly below $\langle \omega_{be} \rangle$ is a point of minor disagreement with the theory, which predicts that the largest growth rates occur for frequencies slightly above $\langle \omega_{be} \rangle$. We have, in fact, observed oscillations at frequencies above $\langle \omega_{be} \rangle$, but at considerably lower amplitude than those at lower frequencies. These high-frequency waves can be easily observed only within a narrow band of ν_{eff}, so that the lower frequency waves are suppressed while the higher frequency waves are still unaffected by collisions. Since waves appear at frequencies both above and below $\langle \omega_{be} \rangle$, it seems likely that the predominance of the latter results from the saturation mechanism rather than from the linear growth rate. The oscillations at frequencies $\omega > \langle \omega_{be} \rangle$ have such high mode numbers that, even though they have higher linear growth rates, they may saturate at lower amplitude than the oscillations at frequencies slightly below $\langle \omega_{be} \rangle$.

The amplitude of even the strongest oscillations is small. Typically $e\tilde{\phi}/T_e \sim 0.01$-0.1%; $\tilde{n}/n \sim 0.1\%$. These relatively low-level fluctuations are to be expected, since the predicted growth rates are small, and, as we shall show, the oscillations are highly localized, high mode number waves that should be susceptible to nonlinear stabilization at low amplitude. The amplitudes that we have observed indicate that for our linear device this particular mode has no significant consequences for enhanced diffusion or energy transport. It is tempting to extend this conclusion to Tokamak geometry, but we must exercise caution in making such an extension, since the saturation mechanism in Tokamaks may be different from that in cylindrical geometry.

We have examined in detail the spatial characteristics of the coherent modes excited in the presence of trapped particles. Figure XII-8 shows crosscorrelation functions taken for a mode at 900 kHz for various azimuthal probe spacings. We observe that the wave propagates azimuthally, and from the correlation data we calculate a mode number $m = 12$. Typically we have observed mode numbers $m \sim 6$-12; in all cases the waves propagate azimuthally in the direction of the electron diamagnetic drift. In Fig. XII-9 we plot mode number as a function of frequency for an extended series of measurements. Also plotted is a calculated best estimate for $\omega = \omega_{*e}$. All measurements were taken under nominally similar conditions, but the parameters necessary for computing ω_{*e} were not monitored continuously; thus, there is perhaps an error of 20% in the calculated curve $\omega = \omega_{*e}$. Also, the difficulty in measuring such small wavelengths results in a ± 1 error for the highest mode numbers. Nevertheless, even with these errors taken into account, the data support the view that $\omega \approx \omega_{*e}$ as predicted by theory.

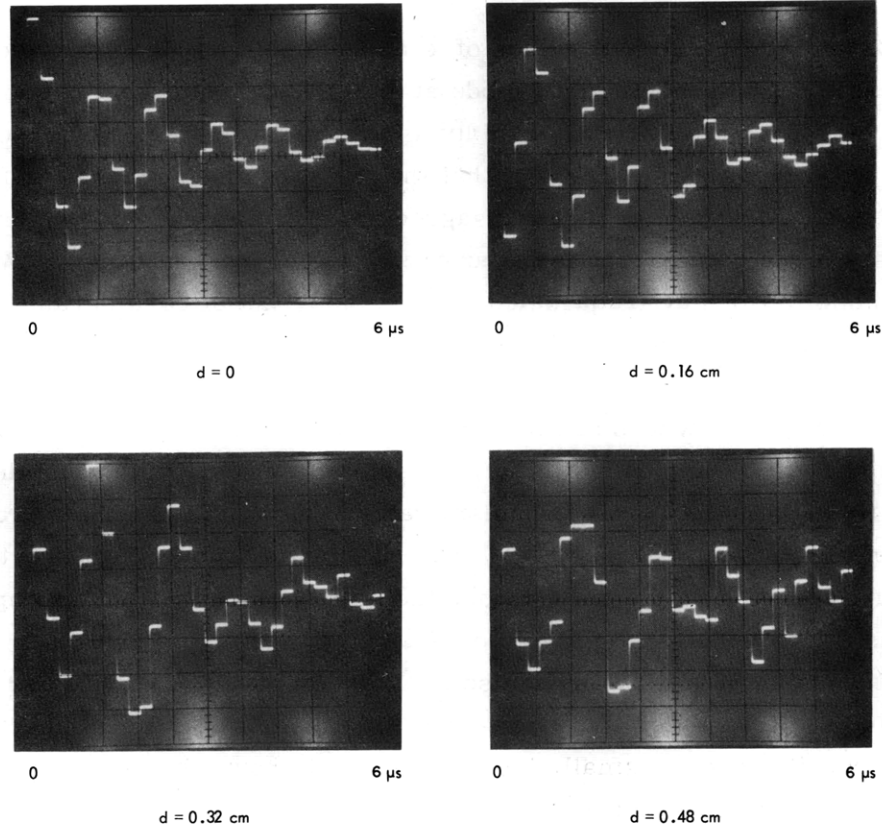We observe that the oscillations are radial standing waves localized within a

Fig. XII-8. Crosscorrelation functions at various azimuthal
spacings, d. r = 0.9 cm, m = 12.

region $\Delta r \sim \dfrac{r}{m}$. The fluctuation amplitude vs radius is shown in Fig. XII-10 where
we have also shown η as a function of radius. The method of plasma production pro-
duces an η profile that has a broad minimum in the range $r \sim 1$-1.5 cm. We find that
the mode amplitude is always peaked in this region of minimum η in agreement with the
theoretical predictions.

The relatively short azimuthal wavelengths $\left(\dfrac{r}{m} \sim 0.5 \text{ cm}\right)$ and strong radial localiza-
tion have hindered efforts to obtain axial phase information. We have measured $\widetilde{\phi}_{rms}$,
however, as a function of z along the entire machine length, and we find that $\widetilde{\phi}_{rms}$ is
periodic in a manner consistent with the assumption that $\widetilde{\phi}_m(z)$ is odd about B_{min}. To
further investigate the axial dependence, we measured the crosscorrelation function
between probes at certain selected axial locations. These data are shown in Fig. XII-11.
As illustrated, probes A and C are located symmetrically across a field maximum,
and probes C and B were located symmetrically across a field minimum. The probes
were carefully aligned along a field line by using emitting probes, and crosscorrelations
were taken between them. We observe that for the pair A, B the crosscorrelation func-
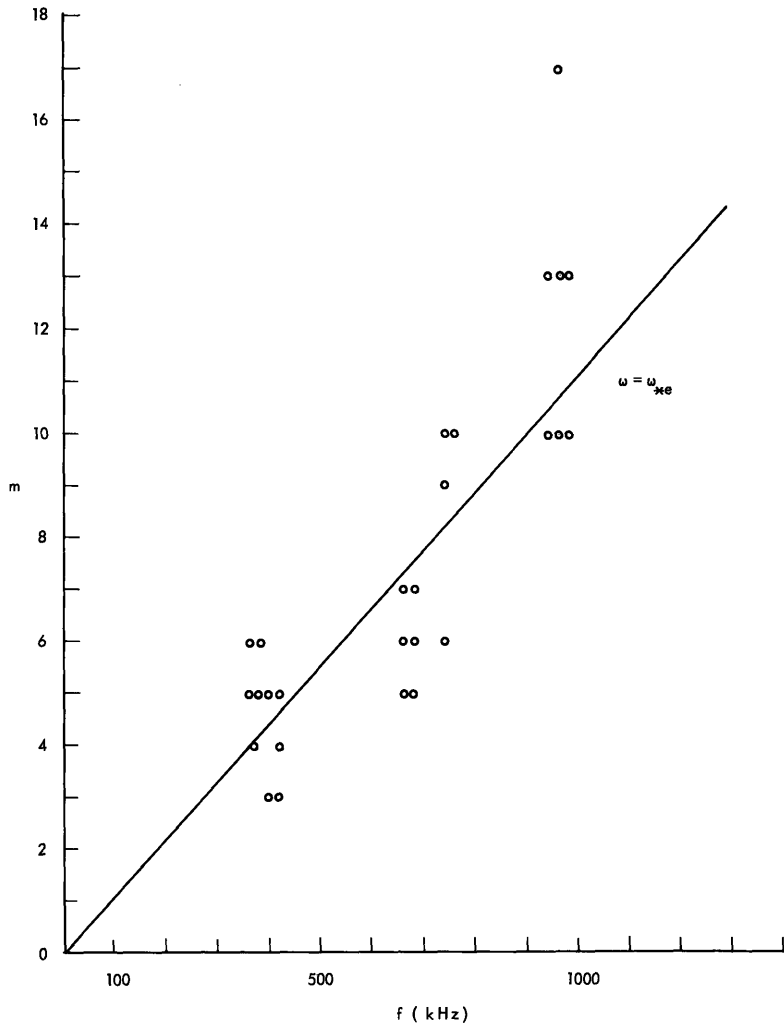tion is the same with B delayed as with A delayed; thus, there is no detectable axial

Fig. XII-9.
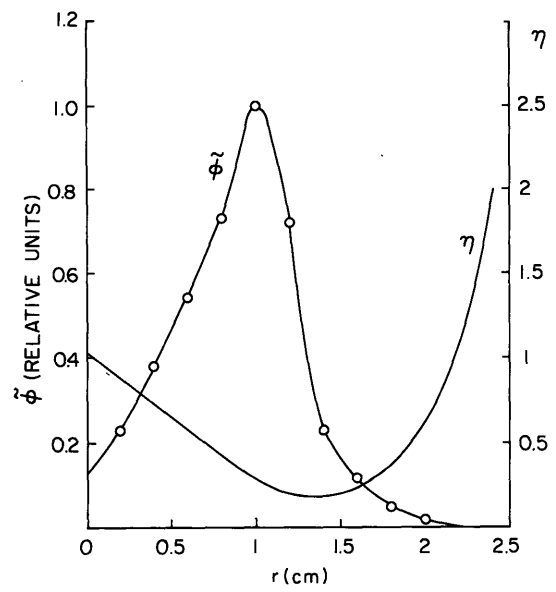
Mode number vs frequency for a series of measurements.

Fig. XII-10.

Amplitude of potential fluctuations vs radius and η vs radius.

0 4 μs 8 μs

A DELAYED WITH RESPECT TO C

0 5 μs 10 μs

B DELAYED WITH RESPECT TO C

0 4 μs 8 μs

C DELAYED WITH RESPECT TO A

0 5 μs 10 μs

C DELAYED WITH RESPECT TO B
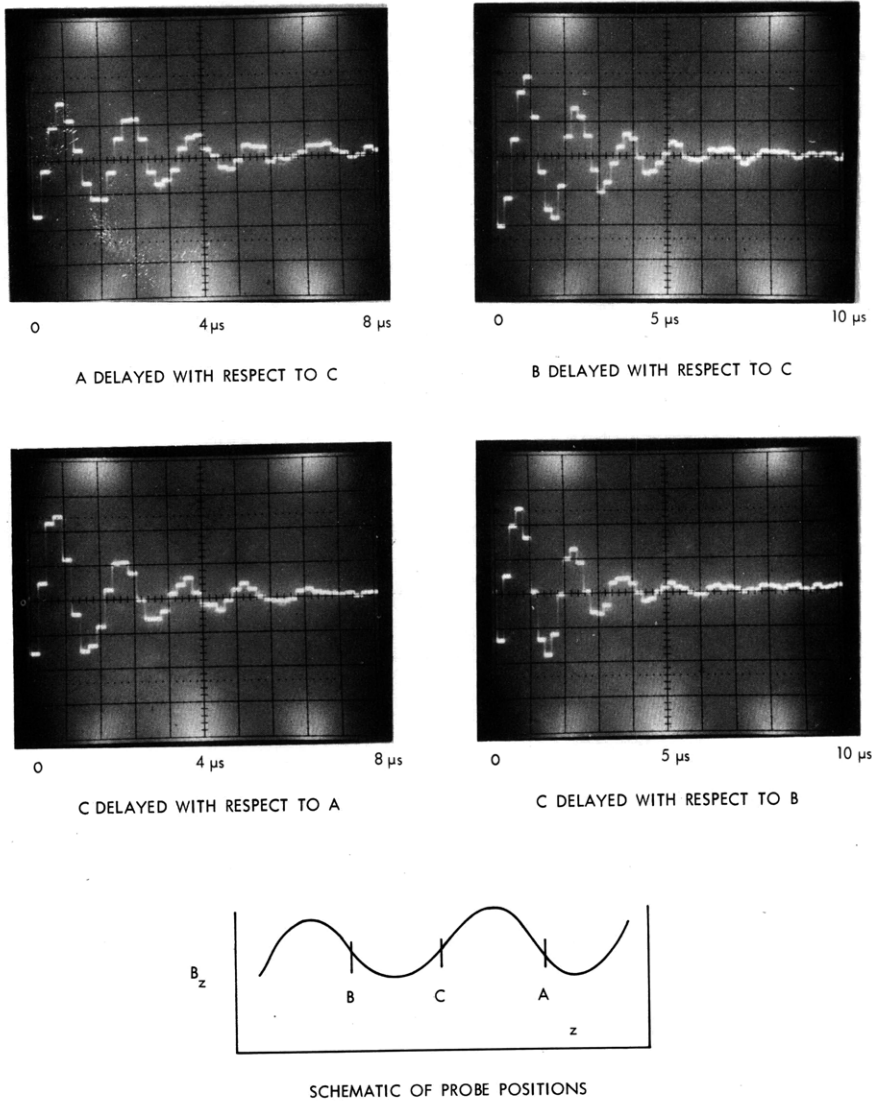
B_z

B C A

z

SCHEMATIC OF PROBE POSITIONS

Fig. XII-11. Axial crosscorrelation functions for probes positioned as shown in the magnetic field.

propagation. But we observe that the potential at A is 180° out of phase from that at B. The results for probes B and C are identical: There is no evidence of axial propagation, but there is a 180° phase shift in the potential between B and C. These results indicate that $\tilde{\phi}_m(z)$ is odd about the field minimum and about the field maximum. The simplest function satisfying these two features is $\tilde{\phi}_m(z) = \sin \frac{2\pi z}{L}$.

We varied the trapping well depth to determine the dependence of wave frequency and
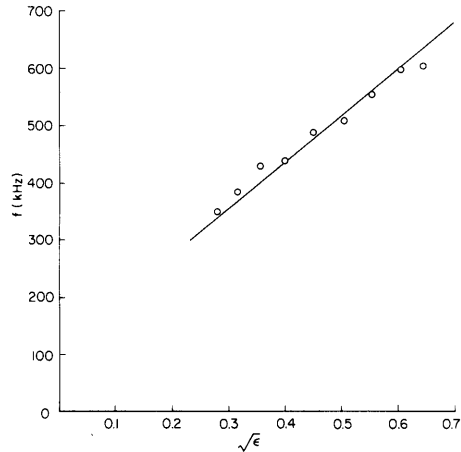

Fig. XII-12. Frequency of the largest amplitude trapped electron wave vs $\sqrt{\epsilon}$.
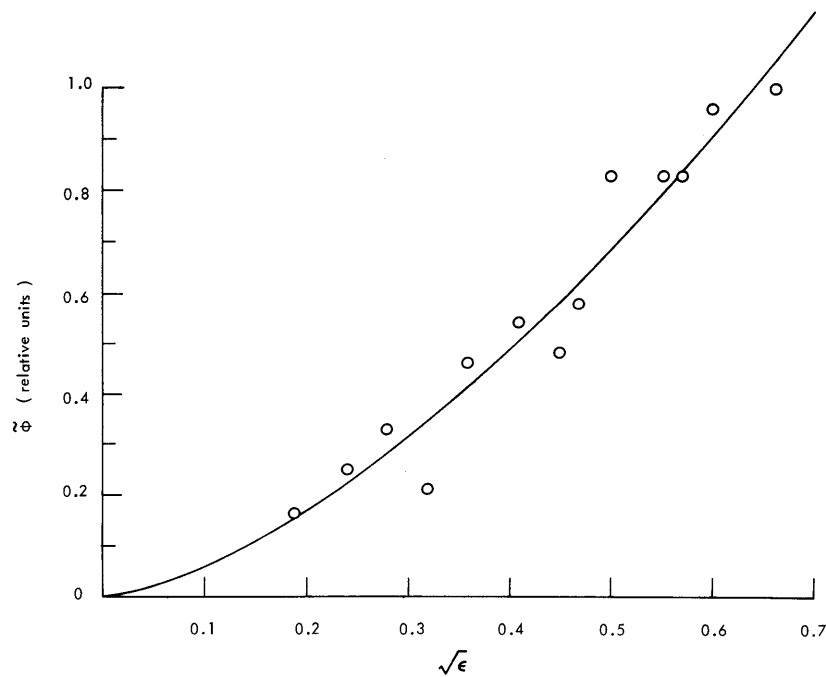

Fig. XII-13. Amplitude of the largest trapped electron wave vs $\sqrt{\epsilon}$. Solid line: a computer generated least-squares fit.

amplitude on ϵ. In Fig. XII-12 we have plotted the frequency of the primary trapped electron mode against $\sqrt{\epsilon}$ for a particular set of machine conditions. We observe that the frequency increases linearly with $\sqrt{\epsilon}$ as predicted from the fact that $\langle \omega_{be} \rangle \propto \sqrt{\epsilon}$. Note, however, that the frequency is not directly proportional to $\sqrt{\epsilon}$, since the curve does not have a zero-frequency intercept. In Fig. XII-13 we have plotted wave amplitude against $\sqrt{\epsilon}$ for a single series of measurements. The dependence on $\sqrt{\epsilon}$ is not so smooth as for the frequency. The scatter in points on the amplitude vs $\sqrt{\epsilon}$ curve results mainly from the shifting mode number as we go to higher $\sqrt{\epsilon}$ and from the difficulty in maintaining identical plasma conditions for the largest values of ϵ. To better determine the amplitude dependence on $\sqrt{\epsilon}$, we did computer generated least-squares fits of the data. The solid curve in Fig. XII-13 is a least-squares fit giving the relation $\tilde{\phi} \propto (\sqrt{\epsilon})^{1.5}$, a dependence that is consistent with theoretical predictions.

Conclusion

We have investigated in cylindrical geometry oscillations occurring at frequencies comparable to the electron bounce frequency. We found that these oscillations are small-amplitude, drift-type waves, propagating in the electron diamagnetic drift direction and having $\omega \approx \omega_{*e}$. The oscillations were observed spatially to be strongly localized radially and to be periodic along the magnetic field. Both amplitude and frequency were found to increase with increasing trapping-well depth. The oscillations are consistent in almost all features with the theoretical predictions for the trapped electron scattering mode in cylindrical geometry. We therefore identify the oscillations as belonging to the trapped electron scattering mode.

References

1. Many papers have been written on the subject of trapped particle modes. Probably the best review paper is B. B. Kadomtsev and O. P. Pogutse, Nucl. Fusion 11, 67 (1971).

2. B. Coppi and G. Rewoldt (in preparation for publication).

3. B. Coppi, Phys. Rev. Letters 29, 1076 (1972).

4. C. W. Horton, Jr., J. D. Callen, and M. N. Rosenbluth, Phys. Fluids 14, 2019 (1971).

XII. PLASMA DYNAMICS

B. General Theory

1. STUDY OF THE FEASIBILITY OF HEATING A TOKAMAK PLASMA BY PARAMETRIC DECAY OF LOW-FREQUENCY ELECTRON PLASMA WAVES

Abraham Bers, Charles F. F. Karney

Introduction

Briggs and Parker[1] have found that it is possible to excite lower hybrid waves in an inhomogeneous plasma with sources at the boundary of the plasma. In a previous report[2] we showed that waves on this branch, but at somewhat higher frequency $\left[\omega^2 \approx \omega_{pi}^2 \left(1 + \dfrac{m_e}{m_i} \cos^2 \theta \right) \approx \omega_{pe}^2 \cos^2 \theta \right]$, can be used as the pump of a parametric interaction and can excite electrostatic ion cyclotron (EIC) waves. In this report we examine the feasibility of using this as a method of heating the plasma of a Tokamak to ignition temperatures.

We shall assume that we can meet the finite pump extent criterion for the interaction, which was outlined previously.[2] Since a nonzero ion temperature causes the EIC waves to ion-cyclotron damp, we shall assume that on the time scale of the discharge (~1 s) all energy converted from lower hybrid frequencies to EIC waves eventually contributes to heating the ions. Strongly nonlinear mechanisms (for example, trapping) may also contribute to ion heating, and thereby considerably shorten the energy transfer time to the ions.

Tokamak Example

We pick an example of a Tokamak that might be typical of a future "scientific feasibility experiment." The parameters that we choose are:

H plasma
R = 6 m
a = 2 m
$n = 10^{14} \text{ cm}^{-3}$
B = 100 kG
T_e = 10 keV
τ = 1 s

In this example $\Omega_i = 9.5 \times 10^8 \text{ s}^{-1}$, $\omega_{pi} = 1.3 \times 10^{10} \text{ s}^{-1}$, $\omega_{pe} = 9.6 \times 10^{11} \text{ s}^{-1}$, $\Omega_e = 1.8 \times 10^{12} \text{ s}^{-1}$, $c_s = 9.8 \times 10^5 \text{ ms}^{-1}$. Our goal is to heat the ions by ΔT_i = 5 keV. This

would correspond to taking the ion temperature from where ohmic heating left off (say, at T_i = 5 keV) to ignition point (~10 keV).

The calculations that follow are under three further assumptions. First, this is the only form of supplementary heating. In an actual experiment it might well be that this form of heating would be used in conjunction with some other method such as neutral injection. Second, these parametric decay processes do not affect the resistivity of the plasma. It may be, however, that the presence of these waves leads to anomalous resistivity and so to additional heating from the plasma current. Third, linear conversion mechanisms (electron damping and wave conversion) are not important. So in these respects we are presenting "worst-case" calculations.

Overall Energy Balance

With these parameters, we find that to heat the ions by ΔT_i in a time τ will require an average power of

$$\frac{n\kappa\Delta T_i \; 2\pi R \; \pi(a/2)^2}{\tau} = 10 \text{ MW}. \tag{1}$$

This is the power that must be provided to the ions. In arriving at this figure we have assumed that only the inner 1/4 of the plasma (radius a/2) is heated. It has been shown[2] that a density gradient does hinder the parametric interactions, and so we expect significant heating only in the central, nearly homogeneous parts of the plasma.

How much power is required in the pump to achieve this power flow into the EIC modes? (Remember that we assume that all energy in the EIC modes goes into heating the ions.) Power in the pump is partitioned between the EIC mode and the idler (another lower hybrid mode) according to the Manley-Rowe relations

$$\frac{P_{idler}}{P_{EIC}} = \frac{\omega_{idler}}{\omega_{EIC}}. \tag{2}$$

Assuming that all the power in the pump is parametrically converted, we have

$$\frac{P_{pump}}{P_{EIC}} = -\frac{\omega_{pump}}{\omega_{EIC}}. \tag{3}$$

(This depletion of the pump's energy is balanced by power flowing into the plasma from the sources.)

A lower limit on pump frequency is set by the requirement that linear wave

conversion does not take place before the center of the plasma. Simonutti and Parker have used the fluid equations,[3] and the results of more recent work with kinetic theory indicate that wave conversion should not take place (for the range of k_z with which we are concerned) as long as

$$\omega_{pump} \gtrsim 2\omega_{LH}. \tag{4}$$

Here, ω_{LH} is the maximum lower hybrid frequency in the plasma. Since $T_i \sim T_e$, ω_{EIC} is normally restricted to lie between the first and second ion cyclotron harmonics,

$$\Omega_i < \omega_{EIC} < 2\Omega_i. \tag{5}$$

For the plasma that we are considering $\omega_{LH} \approx \omega_{pi} \approx 14\,\Omega_i$. So from Eq. 3 we have $P_{pump} \gtrsim 140$ MW in order to get a power flow of 10 MW to the EIC waves. Note, however, that most of this 140 MW would end up in the idler at a frequency a little below the pump frequency. Then it might be possible for the idler to act as a pump. This "cascading" process can continue with the idler of one interaction acting as the pump for the next, until the lower hybrid frequency is reached. If this does happen, the ratio of the power in the EIC waves to that in the pump is increased to

$$\frac{P_{EIC}}{P_{pump}} = -\frac{\omega_{pump} - \omega_{LH}}{\omega_{pump}} \tag{6}$$

So with $\omega_{pump} = 2\omega_{LH}$ we see that we must provide a power P = 20 MW to the pump in the form of RF energy. It might be argued that this coupling to the EIC waves would be more efficient if ω_{pump} were chosen to be greater than $2\omega_{LH}$. But this cascading must be regarded as being somewhat speculative whatever pump frequency is chosen, and 1/2 should probably be considered an upper limit on the fraction of the pump power coupled to EIC waves.

Excitation of the Pump

Briggs and Parker[1] started by assuming an electric field at some small distance ($\sim a\, m_e/m_i$) inside the plasma, where the waves are propagating. In the very low density region the waves are evanescent. Since this region is extremely thin, we assume that the fields at the plasma boundary tunnel into the propagating region with negligible attenuation. We shall assume that the fields at the plasma boundary are imposed by an array of waveguides, as shown in Fig. XII-14. These waveguides support TE_{01} modes with a polarization as shown, and the phase of the mode of each waveguide is shifted by ϕ from the previous phase. The geometry is a planar analog of a Tokamak with the x, y, and z directions corresponding to the radial, poloidal, and toroidal directions. The
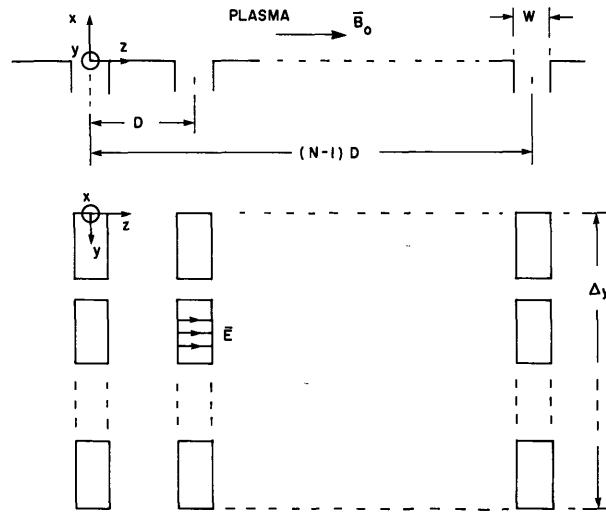
Fig. XII-14. Two views of the waveguide array.

main effect that is not evident with this geometry is the focusing of the RF fields as they propagate toward the center of the plasma.

The field set up in this fashion will have an n_y and n_z of order unity. Inside the plasma a local n_x is defined by the local dispersion relation (in the WKB limit). For lower hybrid waves $n_x \sim \sqrt{m_i/m_e} \gg 1$, and for this reason we neglect the y variation of the fields. The z variation of the fields is given in Fig. XII-15. By Fourier analysis of this field pattern, we obtain its spectrum

$$\left| E_z(k_z) \right| = E_o NW \ \text{sinc}\left(\frac{Wk_z}{2}\right) \frac{\sin \frac{ND}{2}\left(k_z - \frac{\phi}{D}\right)}{N \sin \frac{D}{2}\left(k_z - \frac{\phi}{D}\right)}, \tag{7}$$

where sinc (x) = sin (x)/x. $\left| E_z(k_z) \right|^2$ is sketched in Fig. XII-16.

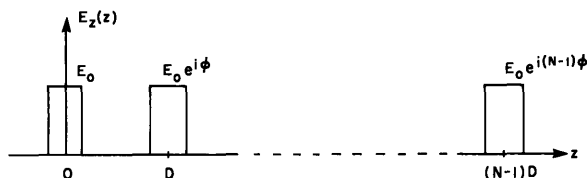Note that we are taking a somewhat simple view of the situation. We assume that

Fig. XII-15. Electric field at x = 0.

the plasma extends right up to the wall of the containing vessel. In reality there would be an appreciable region of effective zero density of thickness (wall radius) − (limiter
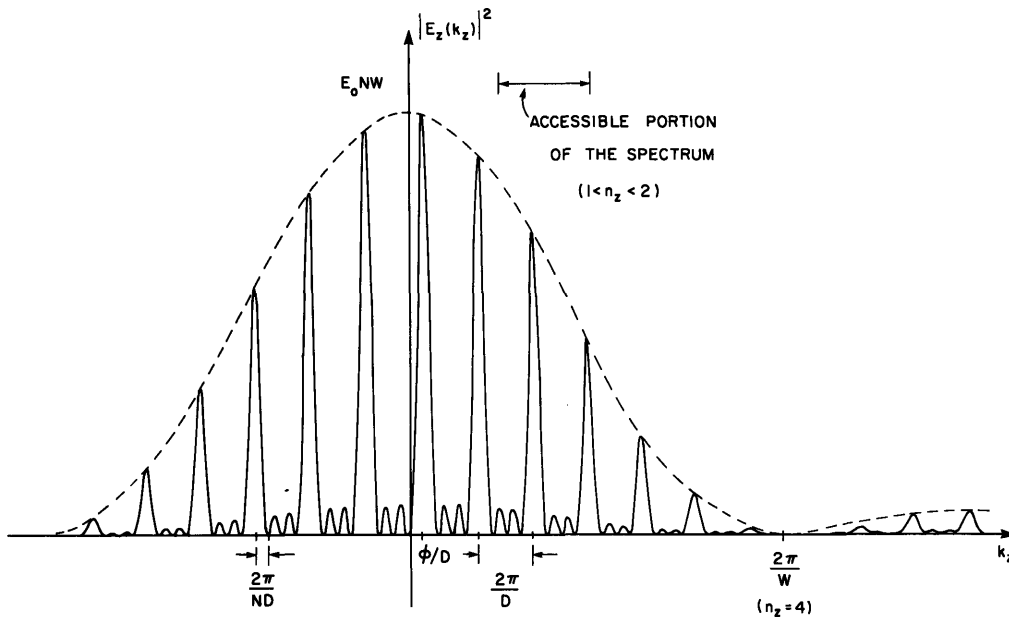
Fig. XII-16. Spectrum of the electric field at x = 0.
($\phi = \pi/2$ and D = 7W.)

radius) which would considerably modify the fields at the plasma boundary. Results of Puri and Tutter[4] suggest that efficient coupling is still possible in this case. The other defect of our excitation scheme is that no attempt is made to match the waveguides to the plasma. Puri and Tutter[5] have proposed a scheme which should stop the plasma from presenting a strongly varying impedance to the waveguide.

In order to choose W we should see what k_z components are going to get into the plasma. On the one hand, we have to satisfy the accessibility condition as given by Parker[6] and others. For plasmas in which $\omega_{pe}^2/\Omega_e^2 \ll 1$ we may take this condition to be

$$n_z = \frac{k_z c}{\omega} > 1. \tag{8}$$

Another restriction on the range of k_z is given by the condition that the pump not be electron Landau damped before reaching the center of the plasma, or

$$\frac{\gamma}{\langle v_{gx} \rangle} a \lesssim 1. \tag{9}$$

Here, v_{gx}, is the x component of the group velocity for these waves which is approximately ω/k, and γ is the damping rate of the mode which is approximately $\omega(\omega/k_z v_{Te})^3 \times \exp\left(-\omega^2/2k_z^2 v_{Te}^2\right)$. With these expressions (9) gives $\omega/k_z v_{Te} > 4$. For the plasma that

we are considering, $c/v_{Te} \simeq 8$. Then (9) gives $n_z < 2$. In order to optimize the fraction of the spectrum of k_z that is admitted, we choose parameters so that the first zero in the envelope occurs at $n_z = 4$, or

$$\frac{2\pi}{W} = \frac{4\omega}{c}.$$ (10)

In this case we note that $W = \lambda_{free\ space}/4$, which is reasonable for the small dimension of a waveguide supporting a TE_{01} mode. If $\omega = 2\omega_{pi}$, (10) gives $W = 1.8$ cm.

We assume then that all k_z satisfying

$$1 < |n_z| < 2$$ (11)

get into the center of the plasma and act as pumps (see Fig. XII-16). For $D \gg W$, the number of peaks in the k_z spectrum that get in (from Eqs. 10 and 11, and Fig. XII-16) is approximately $D/2W$.

Impedance of Plasma

Having determined what waves will get into the plasma, we must calculate how much power they carry. In the quasi-electrostatic approximation the power flow for a single mode in a lossless medium[7] is

$$\bar{S} = -\frac{1}{4} \epsilon_0 |\bar{E}|^2 \omega \left[\frac{(\bar{\bar{K}} + \bar{\bar{K}}_t) \cdot \bar{k}}{k^2} + \frac{k_i k_j}{k^2} \frac{\partial K_{ij}}{\partial \bar{k}} \right].$$ (12)

For a cold plasma K_{ij} is independent of $\bar{k}$, so

$$\frac{\partial}{\partial \bar{k}} K_{ij} = 0.$$ (13)

We are primarily concerned with the power flow in the x direction (that is, from the sources into the center of the plasma).

$$S_x = -\frac{1}{4} \epsilon_0 |\bar{E}|^2 \omega \frac{2K_\perp k_x}{k^2}.$$ (14)

Note that for given S_x, ω, and k_z,

$$|\phi| \sim \frac{1}{\sqrt{K_\perp k_x}} \sim \frac{1}{(K_\perp K_\parallel)^{1/4}},$$ (15)

which is the same as the WKB amplification factor given by Briggs and Parker.[1]

Evaluating (14) near the plasma boundary, say at $\omega_{pe}(x) \gtrsim \omega$, with $K_\perp \approx 1 - \omega_{pi}^2/\omega^2 \approx 1$, $K_\parallel \approx -\omega_{pe}^2/\omega^2 \approx -1$ and $k_x \approx -k_z$, yields

$$S_x = \frac{1}{2} \frac{\omega}{k_z} \epsilon_o |E_z|^2. \tag{16}$$

If we define the impedance of this mode so that

$$S_x = \frac{1}{2} |E_z|^2/Z, \tag{17}$$

then

$$Z = k_z/\epsilon_o \omega. \tag{18}$$

In order to get the x-directed power flow in any part of the spectrum, say, between k_1 and k_2, we perform

$$\int_{k_1}^{k_2} \frac{|E_z(k_z)|^2}{2Z} \frac{dk_z}{2\pi}, \tag{19}$$

where we use the spectrum at $x = 0$. Equation 19 gives the power flow/unit width in the y direction. We perform this integral over the part of the spectrum that is admitted (see Fig. XII-16), that is, for n_z from -2 to -1 and from 1 to 2. As long as N is large, we can split the integral up into a sum of integrals over individual peaks, and assume that the spectrum envelope sinc $(Wk_z/2)$ is constant for each peak. If the ith peak is centered at k_{zi}, the power flow for this peak is approximately

$$\frac{E_o^2 N^2 W^2}{2\pi Z(k_{zi})} \mathrm{sinc}^2 (Wk_{zi}/2) \int_{-\infty}^{\infty} \mathrm{sinc}^2 \left(\frac{ND}{2} k_z\right) dk_z = \frac{NE_o^2 W^2 \epsilon_o \omega}{2D} \frac{\mathrm{sinc}^2 (Wk_{zi}/2)}{k_{zi}}. \tag{20}$$

To perform the sum over peaks we multiply (20) by the number of peaks (D/2W) and replace $\mathrm{sinc}^2 (Wk_{zi}/2)/k_{zi}$ by its value at $k_{zi} = 3\pi/4W$ ($n_z = 3/2$), which for convenience we take to be its average over the sum. Then the x-directed power flow is approximately

$$S_x \approx \frac{NE_o^2 W^2 \epsilon_o \omega}{2D} \frac{D}{2W} \frac{W}{4}$$

$$= \frac{1}{16} NE_o^2 W^2 \epsilon_o \omega \quad \text{(power/unit width in the y direction)}. \tag{21}$$

Size of the Waveguide Array

Now the problem is to see what parameters in (21) will give a total power flow of P = 20 MW. The extent of the waveguide array in the y (poloidal) direction is Δy, and and in the z direction ND. Now P = $S_x \Delta y$, so the area, A, of the waveguide array is given by

$$A = ND\Delta y = ND \frac{P}{S_x} \approx \frac{16PD}{E_o^2 W^2 \epsilon_o \omega}. \tag{22}$$

W was found from (10) to be approximately 1.8 cm. D will normally be determined by such factors as the separation of the magnet coils; we take its value to be 10 cm. We take ω to be twice the lower hybrid frequency or $\sim 2 \times 1.3 \times 10^{10}$ s^{-1}. E_o is determined by factors such as breakdown in the waveguides. It also depends on how well matched the waveguides are to the plasma; if the waveguides see a near short-circuit at their throats, the fields inside the waveguides will be much greater than E_o. Here we take E_o = 1 kV/cm.

Using these numbers in (22), we arrive at a figure of 40 m^2 for A. The total surface area of our Tokamak is $(2\pi R \times 2\pi a) \sim 500$ m^2; so the waveguide array should cover approximately 8% of the area of the Tokamak.

Conclusion

We have shown that it should be possible to heat the ions in a large Tokamak by RF radiation at approximately twice the maximum lower hybrid frequency of the plasma. The energy is coupled into the plasma by a waveguide array that would have to cover approximately 8% of the area of the Tokamak wall. We assume a mechanism for heating that involves parametric coupling to electrostatic ion cyclotron waves, which subsequently ion-cyclotron damp or nonlinearly transfer their energy to the ions.

Two aspects of the calculation leading to this conclusion should be examined in greater detail. One is the possibility of energy "cascading" down in frequency, which we postulate as a mechanism for coupling approximately half of the energy of the pump waves into EIC waves.[8] The second is that we need a detailed knowledge of how best to match a waveguide with a plasma when there is an intervening vacuum layer.

<div align="center">References</div>

1. R. J. Briggs and R. R. Parker, "Transport of RF Energy to the Lower Hybrid Resonance in an Inhomogeneous Plasma," Phys. Rev. Letters 29, 852 (1972).

2. C. F. F. Karney and A. Bers, "Parametric Excitation of Ion Waves by Resonance Cone Fields near the Lower Hybrid Frequency," Quarterly Progress Report No. 113, Research Laboratory of Electronics, M.I.T., April 15, 1974, pp. 105-112.

3. M. D. Simonutti and R. R. Parker, Quarterly Progress Report No. 110, Research Laboratory of Electronics, M. I. T., July 15, 1973, pp. 79-86.

4. S. Puri and M. Tutter, Nucl. Fusion 14, 93 (1974).

5. S Puri and M. Tutter, Z. Naturforsch. 28, 438 (1973).

6. R. R. Parker, Quarterly Progress Report No. 102, Research Laboratory of Electronics, M. I. T., July 15, 1971, pp. 97-111.

7. A. Bers, Notes on Lectures: Linear Waves and Instabilities, given at Ecole d'Eté de Physique Théorique, Les Houches, France, July 1972 (Gordon and Breach, London, in press).

8. The proposed cascading process has been observed recently in an experiment at Princeton: W. M. Hooke, Private communication, June 1974.